
SWIFT: SCALABLE WASSERSTEIN FACTORIZATION FOR SPARSE NONNEGATIVE TENSORS

Ardavan Afshar
Georgia Institute of Technology

Kejing Yin
Hong Kong Baptist University

Sherry Yan
Sutter Health

Cheng Qian
IQVIA

Joyce C. Ho
Emory University

Haesun Park
Georgia Institute of Technology

Jimeng Sun
University of Illinois Urbana-Champaign

ABSTRACT

Existing tensor factorization methods assume that the input tensor follows some specific distribution (i.e. Poisson, Bernoulli and Gaussian), and solve the factorization by minimizing some empirical loss functions defined based on the corresponding distribution. However, it suffers from several drawbacks: 1) In reality, the underlying distributions are complicated and unknown, making it infeasible to be approximated by a simple distribution. 2) The correlation across dimensions of the input tensor is not well utilized, leading to sub-optimal performance. Although heuristics were proposed to incorporate such correlation as side information under Gaussian distribution, they can not easily be generalized to other distributions. Thus, a more principled way of utilizing the correlation in tensor factorization models is still an open challenge. Without assuming any explicit distribution, we formulate the tensor factorization as an *optimal transport* problem with Wasserstein distance, which can handle non-negative inputs.

We introduce *SWIFT*, which minimizes the Wasserstein distance that measures the distance between the input tensor and that of the reconstruction. In particular, we define the N -th order tensor Wasserstein loss for the widely used tensor CP factorization, and derive the optimization algorithm that minimizes it. By leveraging sparsity structure and different equivalent formulations for optimizing computational efficiency, *SWIFT* is as scalable as other well-known CP algorithms. Using the factor matrices as features, *SWIFT* achieves up to 9.65% and 11.31% relative improvement over baselines for downstream prediction tasks. Under the noisy conditions, *SWIFT* achieves up to 15% and 17% relative improvements over the best competitors for the prediction tasks.

1 Introduction

Tensor factorization techniques are effective and powerful tools for analyzing multi-modal data and have been shown tremendous success in a wide range of applications including spatio-temporal analysis [1, 2, 3], graph analysis [4], and health informatics [5, 6] applications. Many constraints such as non-negativity [7], sparsity [8], orthogonality [9], and smoothness [10] are imposed on tensor methods in order to improve the performance both quantitatively and qualitatively. Moreover, depending on the nature of input data, tensor methods fit different distributions on data including Gaussian [11], Poisson [12], Bernoulli [13] distributions and minimize various empirical loss functions such as sum square loss, KL-divergence, and log-loss. However, there are several limitations with these techniques. 1) Existing factorization models often assume some specific data distributions. In practice the underlying distribution are complicated and often unknown. 2) The nature of these factorization models neglects correlation relations among the dimensions in each tensor mode (such as external knowledge about similarity among those features). Although there are several extensions to tensor factorization approaches that consider these similarity matrices as side information [14, 15], they are derived under Gaussian distribution and are not directly generalizable to unknown distributions.

Recent success of *Wasserstein distance or loss* (a.k.a. earth mover’s distance or *optimal transport* distance) shows its potential as a better measure of the difference between two distributions [16, 17, 18]. This distance metric provides a natural measure of the distance between two distribution vectors via a ground metric of choice and can be defined as the cost of the optimal transport plan for moving the mass in the source vector to match that in the target vector. Recently, Wasserstein distance has been applied to matrix factorization and dictionary learning problems with great

success [19, 20, 21, 22, 23]. To our knowledge, its extension to tensor factorization was never studied and is in fact non-trivial due to the following challenges:

- **Wasserstein loss is not well-defined for tensors:** The Wasserstein loss is originally defined over vectors, where each entry of the vector represents one physical location and the cost of transporting from one location to another is used. Existing matrix-based Wasserstein loss are defined by the sum of the vector-based Wasserstein loss over the columns of the matrices [20]. Unfortunately, this definition is not applicable to tensors of multiple modes.
- **Wasserstein loss is difficult to scale:** Learning with Wasserstein loss generally requires solving the optimal transport problem in each iteration, which is extremely time-consuming.
- **Sparse Nonnegative input:** Existing works on Wasserstein matrix factorization assume dense input while real data are often sparse. If designed properly the sparse input can potentially lead to computationally efficient methods.

To overcome these challenges, we propose *SWIFT*, a tensor factorization method which efficiently minimizes Wasserstein distance for sparse nonnegative tensors. The main contributions of *SWIFT* include:

- **Defining Optimal Transport for Tensors that Handles Nonnegative Input:** *SWIFT* is the first technique that minimizes optimal transport (OT) distance for tensor factorization approaches. The benefit of OT is that it does not assume any specific distribution in the data. *SWIFT* is able to handle nonnegative inputs such as binary, counts and probability measures, which are common input in real-world tensor data.
- **Full Utilization of Data Sparsity and Parallelism:** By fully exploring and utilizing the sparsity structure of the input data, *SWIFT* significantly reduces the number of times required to compute OT and enables parallelism. *SWIFT* obtains up to $16\times$ faster OT computation than direct implementation of Wasserstein tensor factorization.
- **Efficient Computation:** *SWIFT* reduces the amount of computations by smartly rearranging the objective function for solving each factor matrix. Scalability of *SWIFT* is comparable with well-known CP algorithms. Moreover, *SWIFT* achieves up to $921\times$ speed up over a direct implementation of Wasserstein tensor factorization without our speedup strategies (Section 6.10 in appendix).

2 Notations and Background

2.1 Basic Notations and Tensor Operations

We denote vectors by bold lowercase letters (*e.g.* \mathbf{u}), matrices by bold uppercase letters (*e.g.* \mathbf{A}), and tensors by Euler script letters (*e.g.* \mathcal{X}). The entropy E for a nonnegative matrix $\mathbf{A} \in \mathbb{R}_+^{M \times N}$ is defined as $E(\mathbf{A}) = -\sum_{i,j=1}^{M,N} \mathbf{A}(i,j) \log(\mathbf{A}(i,j))$. $KL(\mathbf{A}||\mathbf{B})$ is the generalized KL-divergence between two matrices $\mathbf{A}, \mathbf{B} \in \mathbb{R}^{M \times N}$ is defined as $KL(\mathbf{A}||\mathbf{B}) = \sum_{i,j=1}^{M,N} \mathbf{A}(i,j) \log(\frac{\mathbf{A}(i,j)}{\mathbf{B}(i,j)}) - \mathbf{A}(i,j) + \mathbf{B}(i,j)$.

Mode- n Matricization Matricization [24] is the process of reordering the entries of a tensor into a matrix. Specifically, the mode- n matricization is the concatenation of all the mode- n fibers obtained by fixing the indices for every but the n^{th} mode. It transforms the tensor $\mathcal{X} \in \mathbb{R}^{I_1 \times I_2 \times \dots \times I_N}$ into matrix $\mathbf{X}_{(n)}$, and the size of the resulting matrix is I_n by $I_1 \dots I_{n-1} I_{n+1} \dots I_N$. To ease the notation, we define $I_{(-n)} = I_1 \dots I_{n-1} I_{n+1} \dots I_N$.

Khatri-Rao Product The Khatri-Rao product [24] of two matrices $\mathbf{A} \in \mathbb{R}^{I \times R}$ and $\mathbf{B} \in \mathbb{R}^{J \times R}$ is the column-wise Kronecker product $\mathbf{C} = \mathbf{A} \odot \mathbf{B} = [\mathbf{a}_1 \otimes \mathbf{b}_1 \quad \mathbf{a}_2 \otimes \mathbf{b}_2 \quad \dots \quad \mathbf{a}_R \otimes \mathbf{b}_R]$, where $\mathbf{a}_i, \mathbf{b}_i$ are the column- i of matrices \mathbf{A} and \mathbf{B} , \otimes denotes the Kronecker product, and $\mathbf{C} \in \mathbb{R}^{IJ \times R}$. We denote the Khatri-Rao product of all factor matrices except the n -th mode as

$$\mathbf{A}_{\odot}^{(-n)} = (\mathbf{A}_N \odot \dots \odot \mathbf{A}_{n+1} \odot \mathbf{A}_{n-1} \odot \dots \odot \mathbf{A}_1) \in \mathbb{R}^{I_{(-n)} \times R}, \quad (1)$$

where $\mathbf{A}_n \in \mathbb{R}^{I_n \times R}$ indicates the n -th factor matrix.

Canonical/Polyadic (CP) decomposition The CP factorization [24] approximates a tensor \mathcal{X} as the sum of rank-one tensors ($\hat{\mathcal{X}} = \llbracket \mathbf{A}^{(1)}, \mathbf{A}^{(2)}, \dots, \mathbf{A}^{(N)} \rrbracket = \sum_{r=1}^R \mathbf{a}_r^{(1)} \circ \mathbf{a}_r^{(2)} \circ \dots \circ \mathbf{a}_r^{(N)}$), where $\hat{\mathcal{X}}$ is a reconstructed tensor, $\mathbf{a}_r^{(n)}$ is the r -th column of factor matrix $\mathbf{A}^{(n)}$, \circ denotes the outer product of vectors, and R is the number of the rank-one tensors to approximate the input tensor, *i.e.*, the target rank. The mode- n matricization of reconstructed tensor $\hat{\mathcal{X}}$ is $\hat{\mathbf{X}}_{(n)} = \mathbf{A}_n (\mathbf{A}_{\odot}^{(-n)})^T \in \mathbb{R}^{I_n \times I_{(-n)}}$. Table 4 (in the appendix) summarizes the notations and symbols.

2.2 Preliminaries & Related Work

Wasserstein Distance and Optimal Transport Wasserstein distance (*a.k.a.* earth mover’s distance or optimal transport distance) computes the distance between two probability vectors¹. Given two vectors $\mathbf{a} \in \mathbb{R}_+^n$, $\mathbf{b} \in \mathbb{R}_+^m$ and cost matrix $\mathbf{C} \in \mathbb{R}_+^{n \times m}$, the Wasserstein distance between \mathbf{a} , \mathbf{b} is shown by $W(\mathbf{a}, \mathbf{b})$ and minimizes $\langle \mathbf{C}, \mathbf{T} \rangle$ where $\langle \cdot, \cdot \rangle$ indicates the Frobenius inner product and $\mathbf{C} \in \mathbb{R}_+^{n \times m}$ is a symmetric input cost matrix where $\mathbf{C}(i, j)$ represents the cost of moving $\mathbf{a}[i]$ to $\mathbf{b}[j]$. $\mathbf{T} \in U(\mathbf{a}, \mathbf{b})$ where \mathbf{T} is an optimal transport solution between probability vectors \mathbf{a} and \mathbf{b} and $U(\mathbf{a}, \mathbf{b}) = \{\mathbf{T} \in \mathbb{R}_+^{n \times m} | \mathbf{T}\mathbf{1}_n = \mathbf{a}, \mathbf{T}^T\mathbf{1}_m = \mathbf{b}\}$ is a set of all non-negative $n \times m$ matrices with row and column sums \mathbf{a} , \mathbf{b} respectively. $\mathbf{1}_m$ represents m dimensional vector of ones. The aforementioned problem has complexity $O(n^3)$ (assuming $m = n$) [25, 26]. However, computing this distance metric comes with a heavy computational price [27]. In order to reduce the complexity of computation, Cuturi et.al. [17] propose an entropy regularized optimal transport problem between vectors \mathbf{a} , \mathbf{b} :

$$W_V(\mathbf{a}, \mathbf{b}) = \underset{\mathbf{T} \in U(\mathbf{a}, \mathbf{b})}{\text{minimize}} \quad \langle \mathbf{C}, \mathbf{T} \rangle - \frac{1}{\rho} E(\mathbf{T}), \quad (2)$$

where $E(\mathbf{T})$ is an entropy function and ρ is a regularization parameter. When $\rho \geq 0$, the solution of (2) is called the *Sinkhorn divergence* (*a.k.a.* entropy regularized Wasserstein distance) between probability vectors \mathbf{a} and \mathbf{b} . Eq. (2) is a strictly convex problem with a unique solution and can be computed with vectors $\mathbf{u} \in \mathbb{R}_+^n$, $\mathbf{v} \in \mathbb{R}_+^m$ such that $\text{diag}(\mathbf{u})\mathbf{K}\text{diag}(\mathbf{v}) \in U(\mathbf{a}, \mathbf{b})$. Here, $\mathbf{K} = \exp(-\rho\mathbf{C}) \in \mathbb{R}_+^{n \times m}$. Finding the optimal \mathbf{u} and \mathbf{v} can be computed via the Sinkhorn’s algorithm [28].

Wasserstein Dictionary Learning There are several techniques for minimizing Wasserstein loss for dictionary learning problem [19, 20, 21, 22, 23, 29]. Sandler et.al. [19] introduces the first non-negative matrix factorization problem that minimizes Wasserstein loss by proposing a linear programming problem, however, their method needs heavy computation. Cuturi [20] proposed a Wasserstein dictionary learning problem based on entropy regularization. [21] proposes a similar method by exploiting knowledge in both data manifold and features correlation. Xu [29] introduces a nonlinear matrix factorization approach for graphs that considers topological structures. Unfortunately, the direct generalization of these approaches to tensor inputs suffers from the following challenges:

- **Sparse input:** Without carefully exploiting sparsity structure in the input, there will be a huge number of optimal transport problems to be solved for tensor input.
- **Efficient tensor computation:** Updating every factor matrix in Wasserstein tensor problem requires nontrivial tensor operation which can be extremely costly if not optimized.

3 SWIFT Framework

We define and solve optimal transport problem for tensor input by proposing Scalable Wasserstein Factorization (SWIFT) for sparse nonnegative tensors. First we define the input and output for SWIFT. Our proposed method requires the N -th order tensor $\mathcal{X} \in \mathbb{R}^{I_1 \times \dots \times I_N}$ and N cost matrices $\mathbf{C}_n \in \mathbb{R}_+^{I_n \times I_n}$ ($n = 1, \dots, N$) capturing the relations between dimensions along each tensor mode as an **input**. Here, \mathbf{C}_n is a cost matrix for mode n and can be computed directly from the tensor input, or derived from external knowledge. It can also be 1-identity matrix meaning the correlation among features are ignored if the cost matrix is not available. SWIFT is based on CP decomposition and computes N non-negative factor matrices $\mathbf{A}_n \in \mathbb{R}_+^{I_n \times R}$ ($n = 1, \dots, N$) as an **output**. These factor matrices can be used for clustering analysis or other downstream tasks such as input to classification models.

3.1 Wasserstein Distance for Tensors

Definition 1 Wasserstein Matrix Distance: Given a cost matrix $\mathbf{C} \in \mathbb{R}_+^{M \times M}$, the Wasserstein distance between two matrices $\mathbf{A} = [\mathbf{a}_1, \dots, \mathbf{a}_P] \in \mathbb{R}_+^{M \times P}$ and $\mathbf{B} = [\mathbf{b}_1, \dots, \mathbf{b}_P] \in \mathbb{R}_+^{M \times P}$ is denoted by $W_M(\mathbf{A}, \mathbf{B})$, and given by:

$$\begin{aligned} W_M(\mathbf{A}, \mathbf{B}) &= \sum_{p=1}^P W_V(\mathbf{a}_p, \mathbf{b}_p) \\ &= \underset{\mathbf{T}_p \in U(\mathbf{a}_p, \mathbf{b}_p)}{\text{minimize}} \sum_{p=1}^P \langle \mathbf{C}, \mathbf{T}_p \rangle - \frac{1}{\rho} E(\mathbf{T}_p) \\ &= \underset{\mathbf{T} \in U(\mathbf{A}, \mathbf{B})}{\text{minimize}} \langle \mathbf{C}, \mathbf{T} \rangle - \frac{1}{\rho} E(\mathbf{T}), \end{aligned} \quad (3)$$

¹Vector \mathbf{a} is a probability vector if $\|\mathbf{a}\|_1 = 1$ and all elements in \mathbf{a} are non-negative.

Note that sum of the minimization equals minimization of sums since each \mathbf{T}_p is independent of others. Here, ρ is a regularization parameter, $\bar{\mathbf{C}} = \underbrace{[\mathbf{C}, \dots, \mathbf{C}]}_{P \text{ times}}$ and $\bar{\mathbf{T}} = [\mathbf{T}_1, \dots, \mathbf{T}_P]$ are concatenations of the cost matrices and the transport matrices for the P optimal transport problems, respectively. Note that $U(\mathbf{A}, \mathbf{B})$ is the feasible region of the transport matrix $\bar{\mathbf{T}}$ and is given by:

$$\begin{aligned} U(\mathbf{A}, \mathbf{B}) &= \left\{ \bar{\mathbf{T}} \in \mathbb{R}_+^{M \times MP} \mid \mathbf{T}_p \mathbf{1}_M = \mathbf{a}_p, \mathbf{T}_p^T \mathbf{1}_M = \mathbf{b}_p \quad \forall p \right\} \\ &= \left\{ \bar{\mathbf{T}} \in \mathbb{R}_+^{M \times MP} \mid \Delta(\bar{\mathbf{T}}) = \mathbf{A}, \Psi(\bar{\mathbf{T}}) = \mathbf{B} \right\} \end{aligned} \quad (4)$$

where $\Delta(\bar{\mathbf{T}}) = [\mathbf{T}_1 \mathbf{1}_M, \dots, \mathbf{T}_P \mathbf{1}_M] = \bar{\mathbf{T}}(\mathbf{I}_P \otimes \mathbf{1}_M)$, $\Psi(\bar{\mathbf{T}}) = [\mathbf{T}_1^T \mathbf{1}_M, \dots, \mathbf{T}_P^T \mathbf{1}_M]$ and $\mathbf{1}_M$ is a one vector with length M .

Definition 2 Wasserstein Tensor Distance: The Wasserstein distance between N -th order tensor $\mathcal{X} \in \mathbb{R}_+^{I_1 \times \dots \times I_N}$ and its reconstruction $\hat{\mathcal{X}} \in \mathbb{R}_+^{I_1 \times \dots \times I_N}$ is denoted by $W_T(\hat{\mathcal{X}}, \mathcal{X})$:

$$\begin{aligned} W_T(\hat{\mathcal{X}}, \mathcal{X}) &= \sum_{n=1}^N W_M(\hat{\mathbf{X}}_{(n)}, \mathbf{X}_{(n)}) \\ &\equiv \sum_{n=1}^N \left\{ \underset{\bar{\mathbf{T}}_n \in U(\hat{\mathbf{X}}_{(n)}, \mathbf{X}_{(n)})}{\text{minimize}} \quad \langle \bar{\mathbf{C}}_n, \bar{\mathbf{T}}_n \rangle - \frac{1}{\rho} E(\bar{\mathbf{T}}_n) \right\}, \end{aligned} \quad (5)$$

where $\bar{\mathbf{C}}_n = [\mathbf{C}_n, \mathbf{C}_n, \dots, \mathbf{C}_n] \in \mathbb{R}_+^{I_n \times I_n I_{(-n)}}$ is obtained by repeating the cost matrix of the n -th mode for $I_{(-n)}$ times and horizontally concatenating them. $\bar{\mathbf{T}}_n = [\mathbf{T}_{n1}, \dots, \mathbf{T}_{nj}, \dots, \mathbf{T}_{nI_{(-n)}}] \in \mathbb{R}_+^{I_n \times I_n I_{(-n)}}$ and $\mathbf{T}_{nj} \in \mathbb{R}_+^{I_n \times I_n}$ is the transport matrix between the columns $\hat{\mathbf{X}}_{(n)}(:, j) \in \mathbb{R}_+^{I_n}$ and $\mathbf{X}_{(n)}(:, j) \in \mathbb{R}_+^{I_n}$.

Note that $\bar{\mathbf{C}}$ and $\bar{\mathbf{C}}_n$ are for notation convenience and we do not keep multiple copies of \mathbf{C} and \mathbf{C}_n in implementation.

Proposition 1 The Wasserstein distance between tensors \mathcal{X} and \mathcal{Y} denoted by $W_T(\mathcal{X}, \mathcal{Y})$ is a valid distance and satisfies the metric axioms as follows:

1. Positivity: $W_T(\mathcal{X}, \mathcal{Y}) \geq 0$
2. Symmetry: $W_T(\mathcal{X}, \mathcal{Y}) = W_T(\mathcal{Y}, \mathcal{X})$
3. Triangle Inequality: $\forall \mathcal{X}, \mathcal{Y}, \mathcal{Z} \quad W_T(\mathcal{X}, \mathcal{Y}) \leq W_T(\mathcal{X}, \mathcal{Z}) + W_T(\mathcal{Z}, \mathcal{Y})$

We provide the proof in the appendix.

3.2 Wasserstein Tensor Factorization

Given an input tensor \mathcal{X} , SWIFT aims to find the low-rank approximation $\hat{\mathcal{X}}$ such that their Wasserstein distance in (5) is minimized. Formally, we solve for $\hat{\mathcal{X}}$ by minimizing $W_T(\hat{\mathcal{X}}, \mathcal{X})$, where $\hat{\mathcal{X}} = \llbracket \mathbf{A}_1, \dots, \mathbf{A}_N \rrbracket$ is the CP factorization of \mathcal{X} . Together with Definitions 1 and 2, we have the following optimization problem:

$$\begin{aligned} &\underset{\{\mathbf{A}_n \geq 0, \bar{\mathbf{T}}_n\}_{n=1}^N}{\text{minimize}} \quad \sum_{n=1}^N \left(\langle \bar{\mathbf{C}}_n, \bar{\mathbf{T}}_n \rangle - \frac{1}{\rho} E(\bar{\mathbf{T}}_n) \right) \\ &\text{subject to} \quad \hat{\mathcal{X}} = \llbracket \mathbf{A}_1, \dots, \mathbf{A}_N \rrbracket \\ &\quad \quad \quad \bar{\mathbf{T}}_n \in U(\hat{\mathbf{X}}_{(n)}, \mathbf{X}_{(n)}), \quad n = 1, \dots, N \end{aligned} \quad (6)$$

where the first constraint enforces a low-rank CP approximation, the second one ensures that the transport matrices are inside the feasible region. We also interested in imposing non-negativity constraint on the CP factor matrices for both well-definedness of the optimal transport problem and interpretability of the factor matrices. Similar to prior works on vector-based, and matrix-based Wasserstein distance minimization problems [18, 21], in order to handle non-probability inputs, we convert the second hard constraint in (6) to soft regularizations by Lagrangian method using the generalized KL-divergence. Together with the fact that $\hat{\mathbf{X}}_{(n)} = \mathbf{A}_n (\mathbf{A}_{\odot}^{(-n)})^T$ for CP factorization, we convert (6) into the following

objective function:

$$\underset{\{\mathbf{A}_n \geq 0, \bar{\mathbf{T}}_n\}_{n=1}^N}{\text{minimize}} \sum_{n=1}^N \left(\underbrace{\langle \bar{\mathbf{C}}_n, \bar{\mathbf{T}}_n \rangle - \frac{1}{\rho} E(\bar{\mathbf{T}}_n)}_{\text{Part } P_1} + \underbrace{\lambda \left(KL(\Delta(\bar{\mathbf{T}}_n) \| \mathbf{A}_n (\mathbf{A}_{\odot}^{(-n)})^T \right)}_{\text{Part } P_2} + \underbrace{KL(\Psi(\bar{\mathbf{T}}_n) \| \mathbf{X}_{(n)})}_{\text{Part } P_3} \right) \quad (7)$$

where $\Delta(\bar{\mathbf{T}}_n) = [\mathbf{T}_{n1}\mathbf{1}, \dots, \mathbf{T}_{nj}\mathbf{1}, \dots, \mathbf{T}_{nI_{(-n)}}\mathbf{1}]$, $\Psi(\bar{\mathbf{T}}_n) = [\mathbf{T}_{n1}^T\mathbf{1}, \dots, \mathbf{T}_{nj}^T\mathbf{1}, \dots, \mathbf{T}_{nI_{(-n)}}^T\mathbf{1}]$, and λ is the weighting parameter for generalized KL-divergence regularization.

We use the alternating minimization to solve (7). SWIFT iteratively updates: 1) **Optimal Transports Problems**. For each mode- n matricization, SWIFT computes at most a set of $I_{(-n)}$ optimal transport problems. By exploiting the sparsity structure and avoiding explicitly computing transport matrices we can significantly reduce the computation cost. 2) **Factor Matrices**. The CP factor matrices are involved inside the Khatri-Rao product and needs excessive amount of computation. However, by rearranging the terms involved in (7), we can efficiently update each factor matrix. Next, we provide efficient ways to update optimal transport and factor matrices in more details.

3.3 Solution for Optimal Transport Problems

For mode- n , $\bar{\mathbf{T}}_n = [\mathbf{T}_{n1}, \dots, \mathbf{T}_{nj}, \dots, \mathbf{T}_{nI_{(-n)}}] \in \mathbb{R}_+^{I_n \times I_{(-n)}}$ includes a set of $I_{(-n)}$ different optimal transport problems. The optimal solution of j -th optimal transport problem for mode n is $\mathbf{T}_{nj}^* = \text{diag}(\mathbf{u}_j) \mathbf{K}_n \text{diag}(\mathbf{v}_j)$, where $\mathbf{K}_n = e^{(-\rho \mathbf{C}_n - 1)} \in \mathbb{R}_+^{I_n \times I_n}$, $\mathbf{u}_j, \mathbf{v}_j \in \mathbb{R}_+^{I_n}$. This requires computing $I_{(-n)}$ transport matrices with size $I_n \times I_n$ in (7), which is extremely time-consuming. To reduce the amount of computation, SWIFT proposes the following three strategies:

1) Never explicitly computing transport matrices ($\bar{\mathbf{T}}_n^*$): Although we are minimizing (7) with respect to $\bar{\mathbf{T}}_n$, we never explicitly compute $\bar{\mathbf{T}}_n^*$. In stead of directly computing the optimal transport matrices $\bar{\mathbf{T}}_n^*$, we make use of the constraint $\mathbf{T}_{nj}^* \mathbf{1} = \text{diag}(\mathbf{u}_j) \mathbf{K}_n \mathbf{v}_j = \mathbf{u}_j * (\mathbf{K}_n \mathbf{v}_j)$ where $*$ denotes element-wise product. As a result, the following proposition effectively updates objective function 7.

Proposition 2 $\Delta(\bar{\mathbf{T}}_n) = [\mathbf{T}_{n1}\mathbf{1}, \dots, \mathbf{T}_{nj}\mathbf{1}, \dots, \mathbf{T}_{nI_{(-n)}}\mathbf{1}] = \mathbf{U}_n * (\mathbf{K}_n \mathbf{V}_n)$ minimizes (7) where $\mathbf{U}_n = (\hat{\mathbf{X}}_{(n)})^\Phi \odot (\mathbf{K}_n (\mathbf{X}_{(n)} \odot (\mathbf{K}_n^T \mathbf{U}_n)))^\Phi$, $\mathbf{V}_n = (\mathbf{X}_{(n)} \odot (\mathbf{K}_n^T \mathbf{U}_n))^\Phi$, $\Phi = \frac{\lambda \rho}{\lambda \rho + 1}$, and \odot indicates element-wise division. See Section 6.3 for proof.

2) Exploiting Sparsity Structure in $\mathbf{X}_{(n)} \in \mathbb{R}_+^{I_n \times I_{(-n)}}$: We observe that there are many columns with all zero elements in $\mathbf{X}_{(n)}$ due to the sparsity structure in the input data. There is no need to compute transport matrix for those zero columns, therefore, we can easily drop zero value columns in $\mathbf{X}_{(n)}$ and its corresponding columns in $\mathbf{U}_n, \mathbf{V}_n$, and $\hat{\mathbf{X}}_{(n)}$ from our computations. We use NNZ_n to denote the number of non-zero columns in $\mathbf{X}_{(n)}$. By utilizing this observation, we reduce the number of times to solve the optimal transport problems from $I_{(-n)}$ to NNZ_n , where we usually have $NNZ_n \ll I_{(-n)}$ for sparse input.

3) Parallelization of the optimal transport computation: The NNZ_n optimal transport problems for each factor matrix $\mathbf{X}_{(n)}$ can be solved independently. Therefore, parallelization on multiple processes is straightforward for SWIFT. Figure 5 in appendix depicts the computational details of the second and third strategies.

3.4 Solution for Factor Matrices

All the factor matrices are involved in Part P_2 of Objective (7) and present in N different KL-divergence terms. The objective function with respect to factor matrix \mathbf{A}_n for mode n is:

$$\underset{\mathbf{A}_n \geq 0}{\text{minimize}} \sum_{i=1}^N KL(\Delta(\bar{\mathbf{T}}_i) \| \mathbf{A}_i (\mathbf{A}_{\odot}^{(-i)})^T) \quad (8)$$

where $\Delta(\bar{\mathbf{T}}_i) \in \mathbb{R}_+^{I_i \times I_{(-i)}}$, $\mathbf{A}_i \in \mathbb{R}_+^{I_i \times R}$, $\mathbf{A}_{\odot}^{(-i)} \in \mathbb{R}_+^{I_{(-i)} \times R}$. Updating factor matrix \mathbf{A}_n in (8) is expensive due to varying positions of \mathbf{A}_n in the N KL-divergence terms. Specifically, \mathbf{A}_n is involved in the Khatri-Rao product $\mathbf{A}_{\odot}^{(-i)}$, as defined in (1), for every $i \neq n$. On the other hand, when $i = n$, \mathbf{A}_n is not involved in $\mathbf{A}_{\odot}^{(-i)}$.

Efficient rearranging operations In order to solve (8) efficiently, we introduce operator Π , which performs a sequence of reshape, permute and another reshape operations, such that, when applied to the right-hand side of (8), \mathbf{A}_n is no longer involved inside the Khatri-Rao product for all $i \neq n$. Formally,

$$\Pi(\mathbf{A}_i(\mathbf{A}_{\odot}^{(-i)})^T, n) = \mathbf{A}_n(\mathbf{A}_{\odot}^{(-n)})^T \in \mathbb{R}_+^{I_n \times I^{(-n)}} \quad \forall i \neq n. \quad (9)$$

To maintain equivalence to (8), we apply the same operation to the left-hand side of (8), which leads us to the following formulation:

$$\underset{\mathbf{A}_n \geq 0}{\text{minimize}} \quad KL \left(\begin{bmatrix} \Pi(\Delta(\bar{\mathbf{T}}_1), n) \\ \vdots \\ \Pi(\Delta(\bar{\mathbf{T}}_i), n) \\ \vdots \\ \Pi(\Delta(\bar{\mathbf{T}}_N), n) \end{bmatrix} \parallel \begin{bmatrix} \mathbf{A}_n(\mathbf{A}_{\odot}^{(-n)})^T \\ \vdots \\ \mathbf{A}_n(\mathbf{A}_{\odot}^{(-n)})^T \\ \vdots \\ \mathbf{A}_n(\mathbf{A}_{\odot}^{(-n)})^T \end{bmatrix} \right) \quad (10)$$

Where $\Pi(\Delta(\bar{\mathbf{T}}_i), n) \in \mathbb{R}_+^{I_n \times I^{(-n)}}$ for all i . Due to the fact that KL-divergence is computed point-wisely, the above formula is equivalent to (8), with the major difference that \mathbf{A}_n is at the same position in every KL-divergence term in (10), and is no longer involved inside the Khatri-Rao product terms; therefore, it can be much more efficiently updated via multiplicative update rules [30]. More details regarding operator Π , and multiplicative update rules for \mathbf{A}_n are provided in the appendix.

In every iteration of SWIFT, we first update N different optimal transport problems and then update N factor matrices. Algorithm 1 summarizes the optimization procedure in SWIFT.

Proposition 3 *SWIFT is based on Block Coordinate Descent (BCD) algorithm and guarantees convergence to a stationary point. See detailed proofs in the appendix.*

Details regarding complexity analysis are provided in appendix.

Algorithm 1 SWIFT

Input: $\mathcal{X} \in \mathbb{R}_+^{I_1 \times I_2 \times \dots \times I_N}$, $\mathbf{C}_n, NNZ_n \quad n = 1, \dots, N$, target rank R , λ , and ρ

Output: $\mathbf{A}_n \in \mathbb{R}_+^{I_n \times R} \quad n = 1, \dots, N$

```

1:  $\mathbf{K}_n = e^{(-\rho \mathbf{C}_n - 1)}$   $n = 1, \dots, N$ 
2: Initialize  $\mathbf{A}_n \quad n = 1, \dots, N$  randomly.
3: while stopping criterion is not met do
4:   for  $n = 1, \dots, N$  do // Optimal Transport Update (Section 3.3)
5:      $\Phi = \frac{\lambda \rho}{\lambda \rho + 1}$ 
6:      $\mathbf{U}_n = \text{ones}(I_n, NNZ_n) \odot I_n$ 
7:     for  $s=1, \dots, \text{Sinkhorn Iteration}$  do
8:        $\mathbf{U}_n = (\hat{\mathbf{X}}_{(n)})^\Phi \odot \left( \mathbf{K}_n \left( \mathbf{X}_{(n)} \odot (\mathbf{K}_n^T \mathbf{U}_n) \right)^\Phi \right)^\Phi$ 
9:     end for
10:     $\mathbf{V}_n = \left( \mathbf{X}_{(n)} \odot (\mathbf{K}_n^T \mathbf{U}_n) \right)^\Phi$ 
11:     $\Delta(\bar{\mathbf{T}}_n) = \mathbf{U}_n * (\mathbf{K}_n \mathbf{V}_n)$ 
12:  end for
13:  for  $n=1, \dots, N$  do // Factor Matrix Update (Section 3.4)
14:    Update  $\mathbf{A}_n$  based on (10).
15:  end for
16: end while
```

4 Experimental Results

4.1 Experimental Setup

In this section, we answer the following questions:

Q1: Do the factor matrices learned by SWIFT improve downstream classification tasks?

Q2: How is SWIFT's performance on noisy data, compared to existing CP algorithms?

Q3: How scalable is SWIFT compared to existing CP algorithms?

Q4: Are the factor matrices learned by SWIFT interpretable and meaningful?

To enhance the reproducibility of SWIFT, we will provide Matlab implementation of our code after blind reviews.

Dataset Description and Evaluation Metrics

BBC News Classification dataset [31] is a publicly available dataset from the BBC News Agency for text classification task. A third-order count tensor is constructed with the size of 400 articles by 100 words by 100 words. $\mathcal{X}(i, j, k)$ is the number of co-occurrences of the j -th and the k -th words in every sentence of the i -th article. We use the pair-wise cosine distance as the word-by-word and article-by-article cost matrices with details provided in the appendix. The downstream task is to predict the category (from business, entertainment, politics, sport or tech) of each article and we use *accuracy* as the evaluation metric.

Large Health Provider Network (H1) is a dataset collected from a large real-world health provider network containing the electronic health records (EHRs) of patients. A third-order binary tensor is constructed with the size of 1000 patients by 100 diagnoses by 100 medications. The downstream task is to predict the onset of heart failure (HF) for the patients (200 out of the 1000 patients are diagnosed with HF) and use PR-AUC (Area Under the Precision-Recall Curve) to evaluate the HF prediction task.

We chose these two datasets because of different data types (count in BBC, binary in H1). Note that **the cost matrices are derived from the original input by cosine similarity without any additional external knowledge**. Hence the comparisons are fair since the input are the same.

Baselines

We compare the performance of SWIFT with different tensor factorization methods with different loss functions and their variants:

- The first loss function minimizes sum square loss and has 4 variants: 1) **CP-ALS** [11]; 2) **CP-NMU** [11]; 3) **Supervised CP** [15]; and 4) **Similarity based CP** [15]. The first one is unconstrained, the second one incorporates non-negativity constraint, the third one utilizes label information, and the last one uses similarity information among features (similar to SWIFT).
- The second loss function is Gamma loss (**CP-Continuous** [13]) which is the start of the art method (SOTA) for non-negative continuous tensor.
- The third loss function is Log-loss (**CP-Binary** [13]) which is SOTA binary tensor factorization by fitting Bernoulli distribution.
- The fourth loss function is Kullback-Leibler Loss (**CP-APR** [12]) which fits Poisson distribution on the input data and is suitable for count data.

Table 1: The first part reports the average and standard deviation of *accuracy* on the test set as for different value of R on BBC NEWS data. The second part depicts the average and standard deviation of *PR-AUC Score* on test data for H1 dataset. Both experiments are based on five-fold cross validation. We used Lasso Logistic Regression as a classifier.

		R=5	R=10	R=20	R=30	R=40
BBC NEWS Data	CP-ALS [11]	.521 ± .033	.571 ± .072	.675 ± .063	.671 ± .028	.671 ± .040
	CP-NMU [11]	.484 ± .039	.493 ± .048	.581 ± .064	.600 ± .050	.650 ± .031
	Supervised CP [15]	.506 ± .051	.625 ± .073	.631 ± .050	.665 ± .024	.662 ± .012
	Similarity Based CP [15]	.518 ± .032	.648 ± .043	.638 ± .021	.662 ± .034	.673 ± .043
	CP Continuous [13]	.403 ± .051	.481 ± .056	.528 ± .022	.559 ± .024	.543 ± .043
	CP Binary [13]	.746 ± .058	.743 ± .027	.737 ± .008	.756 ± .062	.743 ± .044
	CP-APR [12]	.675 ± .059	.768 ± .033	.753 ± .035	.743 ± .033	.746 ± .043
	SWIFT	.759 ± .013	.781 ± .013	.803 ± .010	.815 ± .005	.818 ± .022
H1 Data	CP-ALS [11]	.327 ± .072	.333 ± .064	.311 ± .068	.306 ± .065	.332 ± .098
	CP-NMU [11]	.300 ± .054	.294 ± .064	.325 ± .085	.344 ± .068	.302 ± .071
	Supervised CP [15]	.301 ± .044	.305 ± .036	.309 ± .054	.291 ± .037	.293 ± .051
	Similarity Based CP [15]	.304 ± .042	.315 ± .041	.319 ± .063	.296 ± .041	.303 ± .032
	CP Continuous [13]	.252 ± .059	.237 ± .043	.263 ± .065	.244 ± .053	.256 ± .077
	CP Binary [13]	.301 ± .061	.325 ± .079	.328 ± .080	.267 ± .074	.296 ± .063
	CP-APR [12]	.305 ± .075	.301 ± .068	.290 ± .052	.313 ± .082	.304 ± .086
	SWIFT	.364 ± .063	.350 ± .031	.350 ± .040	.369 ± .066	.374 ± .044

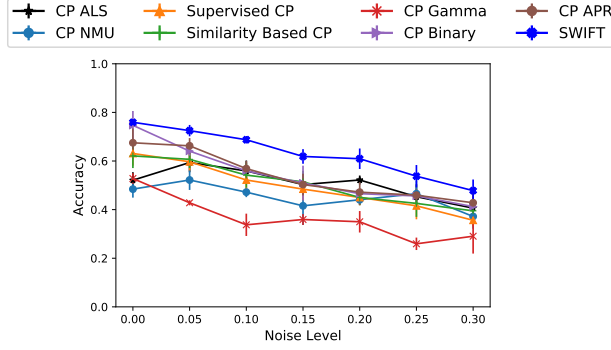


Figure 1: The average and standard deviation of accuracy of different baselines as a function of the noise level on BBC NEWS. SWIFT outperforms other baselines by improving accuracy up to 15%.

4.2 Q1. Classification Performance of SWIFT.

To evaluate low-rank factor matrices, we utilize the downstream prediction tasks as a proxy to assess the performance of SWIFT and the baselines, similar to the existing works [32, 5, 33, 34]. We performed 5-fold cross validation and split the data into training, validation, and test sets by a ratio of 3:1:1. See details of the training strategy and hyper-parameter tuning in the appendix.

Outperforming various tensor factorizations: Table 1 summarizes the classification performance using the factor matrices obtained by SWIFT and the baselines with varying target rank ($R \in \{5, 10, 20, 30, 40\}$). We report the mean and standard deviation of *accuracy* for BBC News, and that of *PR-AUC Score* for H1 dataset on the test set by performing five-fold cross validation. For the BBC News dataset, SWIFT outperforms all the baselines for different target ranks with relative improvement ranging from 1.69% to 9.65%. For the H1 dataset, SWIFT significantly outperforms all baselines for all values of R with relative improvement ranging from 5.10% to 11.31%.

Outperforming various classifiers We compare performance of SWIFT with well-known classifiers on raw data. For BBC data, we matricize along article mode and use word \times word as features. Similarly, for H1 data, we matricize along the patient mode and use medication \times diagnosis as features. Table 2 presents the mean and standard deviation of accuracy and PR-AUC score from Lasso Logistic Regression, Random Forest, Multi-Layer Perceptron, and K-Nearest Neighbor on both BBC NEWS and H1 data sets. It clearly shows that SWIFT using Lasso LR classifier even with $R=5$ outperforms all the other classifiers.

Table 2: Average and standard deviation of accuracy on BBC NEWS and PR-AUC score on H1 data sets by performing Lasso LR, RF, MLP, and KNN on raw data sets.

	Accuracy on BBC	PR-AUC Score on H1
Lasso LR	.728 \pm .013	.308 \pm .033
RF	.6281 \pm .049	.318 \pm .083
MLP	.690 \pm .052	.305 \pm .054
KNN	.5956 \pm .067	.259 \pm .067
SWIFT (R=5)	.759 \pm .013	.364 \pm .063
SWIFT (R=40)	.818 \pm .020	.374 \pm .044

4.3 Q2. Classification Performance on Noisy Data

Noisy Data Construction: To measure the performance of SWIFT against noisy input, we inject noise to the raw input tensor to construct the noisy input tensor. For the binary tensor input, we add Bernoulli noise. Given the noise level (p), we randomly choose zero elements, such that the total number of selected zero elements equals to the number of non-zero elements. Then, we flip the selected zero elements to one with probability p . We follow the similar procedure for the count tensor input, except that we add Poisson noise by flipping the selected zero value to a count value with probability p , and the added noise value is selected uniformly at random between 1 and maximum value in the tensor input.

Performance on BBC data with Noise: Figure 1 presents the average and standard deviation of categorizing the articles on the test data for five-fold cross validation with respect to different levels of noise ($p \in$

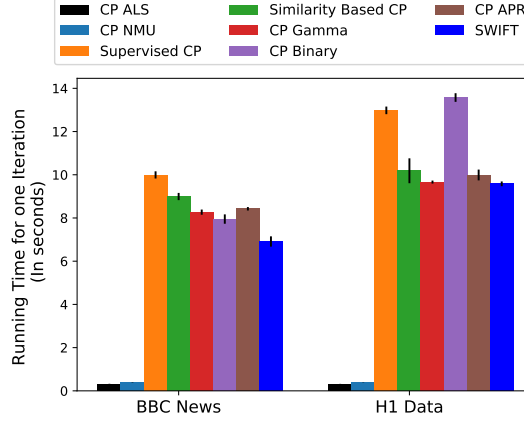


Figure 2: The average and standard deviation of running time in seconds for one iteration as an average of 5 on BBC News and H1 and Data sets by setting $R = 40$ for SWIFT and other well-known Tensor baselines.

$\{0.05, 0.1, 0.15, 0.20, 0.25, 0.30\}$). For all different amounts of noise, SWIFT outperforms other baselines by improving accuracy up to 15% over the best baseline especially for medium and high noise levels. Similar results are achieved in H1 data showing in the appendix.

4.4 Q3. Scalability of SWIFT

In this section, we assess the scalability of SWIFT in comparison to the other 7 CP algorithms introduced earlier. Figure 2 depicts the average and standard deviation of running time in seconds (as an average of 5) for one iteration by setting $R = 40$. In order to have fair comparisons, we switched off the parallelization of the optimal transport computation for SWIFT since none of the baselines utilize parallelization. As shown in Figure 2, SWIFT is as scalable as other baselines, however it improves the performance in both data set suggesting the strategies we introduced in Section 3 make SWIFT scalable. We fixed the parameters to those that we learned in Section 4.2. Scalability of SWIFT in compare to a direct implementation of Wasserstein tensor factorization is provided in Section 6.10 in the appendix.

4.5 Q4. Interpretability of SWIFT

To verify the interpretability of results produced by SWIFT we perform computational phenotyping on H1 data.

Computational phenotyping is a fundamental task in healthcare which refers on extracting meaningful and interpretable medical concepts (patient clusters) from noisy electronic health records (EHRs) [35]. Tensor factorization techniques are powerful tools for extracting meaningful phenotyping [32, 36, 37, 33, 34]. Here we extract heart failure (HF) phenotypes from H1 data set. We use the same tensor as we described in the previous section and run SWIFT by selecting $R = 40$ since it achieves the highest PR-AUC in comparison to other values of R . $\mathbf{A}_2(:, r)$, $\mathbf{A}_3(:, r)$ represent the membership value of diagnosis and medication features in r -th phenotype.

Results: Table 3 presents three phenotype examples. The weight next to phenotype index indicates the lasso logistic regression coefficient for heart failure prediction (e.g., 21.93, 19.58 and -16.22 in Table 3). “Dx” indicates diagnoses and “Rx” represents medications. Every phenotype is clinically meaningful, endorsed and annotated by a medical expert. The first phenotype is about Atrial Fibrillation which captures patients with hypertension and cardiac dysrhythmias that are prescribed high blood pressure medications. Cardiometabolic disease is another phenotype that captures diabetes patients with hypertension. These two phenotypes have high positive weights (21.93 and 19.58 respectively) for predicting HF diagnosis. The third phenotype is depressive and menopausal disorders, Serotonin and Benzodiazepines appeared in this phenotype also are prescribed for these diagnosis codes in the clinical practice. This phenotype has a negative association with HF (weight = -16.22). The remaining phenotypes positively associated with HF are listed in the appendix.

5 Conclusion

We propose Wasserstein Tensor Factorization for sparse nonnegative input data. We introduce several approaches to accelerate the computation for both optimal transport and factor matrix updates by proposing SWIFT. Experimental

Table 3: Three phenotypes examples learned on H1 data set with SWIFT. The weight value for each phenotype represents the lasso logistic regression coefficient for the heart failure prediction task. “Dx” represents for diagnoses and “Rx” indicates for medications. All phenotypes are considered clinically meaningful by a clinical expert.

Atrial Fibrillation (Weight= 21.93)
Dx-Essential hypertension [98.]
Dx-Disorders of lipid metabolism [53.]
Dx-Cardiac dysrhythmias [106.]
Rx-Calcium Channel Blockers
Rx-Alpha-Beta Blockers
Rx-Angiotensin II Receptor Antagonists
Cardiometabolic Disease (Weight= 19.58)
Dx-Diabetes mellitus without complication [49.]
Dx-Essential hypertension [98.]
Dx-Disorders of lipid metabolism [53.]
Rx-Diagnostic Tests
Rx-Biguanides
Rx-Diabetic Supplies
Mental Disorder (Weight= -16.22)
Dx-Anxiety disorders [651]
Dx-Menopausal disorders [173.]
Dx-Depressive disorders [6572]
Rx-Benzodiazepines
Rx-Selective Serotonin Reuptake Inhibitors (SSRIs)
Rx-Serotonin Modulators

results depict that SWIFT outperforms other well-known baselines on downstream classification task for both binary and count tensor inputs. In the presence of noise, SWIFT outperforms other competitors. Moreover the scalability of SWIFT is comparable with other well-known CP algorithms. For the future direction, applying Wasserstein loss to Tucker, and PARAFAC2 decomposition would be interesting.

References

- [1] Mohammad Taha Bahadori, Qi Rose Yu, and Yan Liu. Fast multivariate spatio-temporal analysis via low rank tensor learning. In *Advances in neural information processing systems*, pages 3491–3499, 2014.
- [2] Ardavan Afshar, Joyce C Ho, Bistra Dilkina, Ioakeim Perros, Elias B Khalil, Li Xiong, and Vaidy Sunderam. Cp-ortho: An orthogonal tensor factorization framework for spatio-temporal data. In *Proceedings of the 25th ACM SIGSPATIAL International Conference on Advances in Geographic Information Systems*, pages 1–4, 2017.
- [3] Hadi Fanaee-T and Joao Gama. Event detection from traffic tensors: A hybrid model. *Neurocomputing*, 203:22–33, 2016.
- [4] Ekta Gujral, Ravdeep Pasricha, and Evangelos Papalexakis. Beyond rank-1: Discovering rich community structure in multi-aspect graphs. In *Proceedings of The Web Conference 2020*, pages 452–462, 2020.
- [5] Kejing Yin, Dong Qian, William K Cheung, Benjamin CM Fung, and Jonathan Poon. Learning phenotypes and dynamic patient representations via rnn regularized collective non-negative tensor factorization. In *Proceedings of the AAAI Conference on Artificial Intelligence*, volume 33, pages 1246–1253, 2019.
- [6] Huan He, Jette Henderson, and Joyce C Ho. Distributed tensor decomposition for large scale health analytics. In *The World Wide Web Conference*, pages 659–669, 2019.
- [7] Jingu Kim, Yunlong He, and Haesun Park. Algorithms for nonnegative matrix and tensor factorizations: A unified view based on block coordinate descent framework. *Journal of Global Optimization*, 58(2):285–319, 2014.
- [8] Jette Henderson, Joyce C Ho, Abel N Kho, Joshua C Denny, Bradley A Malin, Jimeng Sun, and Joydeep Ghosh. Granite: Diversified, sparse tensor factorization for electronic health record-based phenotyping. In *2017 IEEE international conference on healthcare informatics (ICHI)*, pages 214–223. IEEE, 2017.
- [9] Yichen Wang, Robert Chen, Joydeep Ghosh, Joshua C Denny, Abel Kho, You Chen, Bradley A Malin, and Jimeng Sun. Rubik: Knowledge guided tensor factorization and completion for health data analytics. In *Proceedings of the 21th ACM SIGKDD International Conference on Knowledge Discovery and Data Mining*, pages 1265–1274, 2015.
- [10] Ardavan Afshar, Ioakeim Perros, Evangelos E Papalexakis, Elizabeth Searles, Joyce Ho, and Jimeng Sun. Copa: Constrained parafac2 for sparse & large datasets. In *Proceedings of the 27th ACM International Conference on Information and Knowledge Management*, pages 793–802, 2018.
- [11] Brett W Bader and Tamara G Kolda. Efficient matlab computations with sparse and factored tensors. *SIAM Journal on Scientific Computing*, 30(1):205–231, 2007.
- [12] Eric C Chi and Tamara G Kolda. On tensors, sparsity, and nonnegative factorizations. *SIAM Journal on Matrix Analysis and Applications*, 33(4):1272–1299, 2012.
- [13] David Hong, Tamara G Kolda, and Jed A Duersch. Generalized canonical polyadic tensor decomposition. *SIAM Review*, 62(1):133–163, 2020.
- [14] Evrim Acar, Tamara G Kolda, and Daniel M Dunlavy. All-at-once optimization for coupled matrix and tensor factorizations. *arXiv preprint arXiv:1105.3422*, 2011.
- [15] Yejin Kim, Robert El-Kareh, Jimeng Sun, Hwanjo Yu, and Xiaoqian Jiang. Discriminative and distinct phenotyping by constrained tensor factorization. *Scientific reports*, 7(1):1114, 2017.
- [16] Martin Arjovsky, Soumith Chintala, and Léon Bottou. Wasserstein generative adversarial networks. In Doina Precup and Yee Whye Teh, editors, *Proceedings of the 34th International Conference on Machine Learning*, volume 70 of *Proceedings of Machine Learning Research*, pages 214–223, International Convention Centre, Sydney, Australia, 06–11 Aug 2017. PMLR.
- [17] Marco Cuturi. Sinkhorn distances: Lightspeed computation of optimal transport. In *Advances in neural information processing systems*, pages 2292–2300, 2013.
- [18] Charlie Frogner, Chiyuan Zhang, Hossein Mobahi, Mauricio Araya, and Tomaso A Poggio. Learning with a wasserstein loss. In *Advances in Neural Information Processing Systems*, pages 2053–2061, 2015.
- [19] Roman Sandler and Michael Lindenbaum. Nonnegative matrix factorization with earth mover’s distance metric. In *2009 IEEE Conference on Computer Vision and Pattern Recognition*, pages 1873–1880. IEEE, 2009.
- [20] Antoine Rolet, Marco Cuturi, and Gabriel Peyré. Fast dictionary learning with a smoothed wasserstein loss. In *Artificial Intelligence and Statistics*, pages 630–638, 2016.
- [21] Wei Qian, Bin Hong, Deng Cai, Xiaofei He, Xuelong Li, et al. Non-negative matrix factorization with sinkhorn distance. In *IJCAI*, pages 1960–1966, 2016.

- [22] Morgan A Schmitz, Matthieu Heitz, Nicolas Bonneel, Fred Ngole, David Coeurjolly, Marco Cuturi, Gabriel Peyré, and Jean-Luc Starck. Wasserstein dictionary learning: Optimal transport-based unsupervised nonlinear dictionary learning. *SIAM Journal on Imaging Sciences*, 11(1):643–678, 2018.
- [23] Erdem Varol, Amin Nejatbakhsh, and Conor McGrory. Temporal wasserstein non-negative matrix factorization for non-rigid motion segmentation and spatiotemporal deconvolution. *arXiv preprint arXiv:1912.03463*, 2019.
- [24] Tamara G Kolda and Brett W Bader. Tensor decompositions and applications. *SIAM Review*, 51(3):455–500, 2009.
- [25] Gabriel Peyré, Marco Cuturi, et al. Computational optimal transport. *Foundations and Trends® in Machine Learning*, 11(5-6):355–607, 2019.
- [26] Yujia Xie, Xiangfeng Wang, Ruijia Wang, and Hongyuan Zha. A fast proximal point method for computing exact wasserstein distance. In *Uncertainty in Artificial Intelligence*, pages 433–453. PMLR, 2020.
- [27] Ofir Pele and Michael Werman. Fast and robust earth mover’s distances. In *2009 IEEE 12th International Conference on Computer Vision*, pages 460–467. IEEE, 2009.
- [28] Richard Sinkhorn and Paul Knopp. Concerning nonnegative matrices and doubly stochastic matrices. *Pacific Journal of Mathematics*, 21(2):343–348, 1967.
- [29] Hongteng Xu. Gromov-wasserstein factorization models for graph clustering. In *AAAI*, pages 6478–6485, 2020.
- [30] Daniel D Lee and H Sebastian Seung. Algorithms for non-negative matrix factorization. In *Advances in neural information processing systems*, pages 556–562, 2001.
- [31] Derek Greene and Pádraig Cunningham. Practical solutions to the problem of diagonal dominance in kernel document clustering. In *Proc. 23rd International Conference on Machine learning (ICML’06)*, pages 377–384. ACM Press, 2006.
- [32] Joyce C Ho, Joydeep Ghosh, and Jimeng Sun. Marble: high-throughput phenotyping from electronic health records via sparse nonnegative tensor factorization. In *Proceedings of the 20th ACM SIGKDD international conference on Knowledge discovery and data mining*, pages 115–124, 2014.
- [33] Ardavan Afshar, Ioakeim Perros, Haesun Park, Christopher deFilippi, Xiaowei Yan, Walter Stewart, Joyce Ho, and Jimeng Sun. Taste: temporal and static tensor factorization for phenotyping electronic health records. In *Proceedings of the ACM Conference on Health, Inference, and Learning*, pages 193–203, 2020.
- [34] Kejing Yin, Ardavan Afshar, Joyce C Ho, William K Cheung, Chao Zhang, and Jimeng Sun. Logpar: Logistic parafac2 factorization for temporal binary data with missing values. In *Proceedings of the 26th ACM SIGKDD International Conference on Knowledge Discovery & Data Mining*, pages 1625–1635, 2020.
- [35] Rachel L Richesson, Jimeng Sun, Jyotishman Pathak, Abel N Kho, and Joshua C Denny. Clinical phenotyping in selected national networks: demonstrating the need for high-throughput, portable, and computational methods. *Artificial intelligence in medicine*, 71:57–61, 2016.
- [36] Kejing Yin, William K Cheung, Yang Liu, Benjamin CM Fung, and Jonathan Poon. Joint learning of phenotypes and diagnosis-medication correspondence via hidden interaction tensor factorization. In *IJCAI*, pages 3627–3633, 2018.
- [37] Juan Zhao, Yun Zhang, David J Schlueter, Patrick Wu, Vern Eric Kerchberger, S Trent Rosenbloom, Quinn S Wells, QiPing Feng, Joshua C Denny, and Wei-Qi Wei. Detecting time-evolving phenotypic topics via tensor factorization on electronic health records: Cardiovascular disease case study. *Journal of biomedical informatics*, 98:103270, 2019.
- [38] Dimitri P Bertsekas. Nonlinear programming. *Journal of the Operational Research Society*, 48(3):334–334, 1997 Section 3.7.
- [39] Stephen Boyd, Stephen P Boyd, and Lieven Vandenberghe. *Convex optimization*. Cambridge university press, 2004.
- [40] Heinz Neudecker. Some theorems on matrix differentiation with special reference to kronecker matrix products. *Journal of the American Statistical Association*, 64(327):953–963, 1969.
- [41] Florian Roemer. *Advanced algebraic concepts for efficient multi-channel signal processing*. PhD thesis, 2012.
- [42] Marco Cuturi and David Avis. Ground metric learning. *The Journal of Machine Learning Research*, 15(1):533–564, 2014.

6 Appendix

The appendix has the following structure: Section 6.1 demonstrates the symbols and notations used throughout this paper. We prove that Wasserstein for tensors is a valid metric and satisfies the metric axioms in Section 6.2. We show that $\Delta(\bar{\mathbf{T}}_n) = [\mathbf{T}_{n1}\mathbf{1}, \dots, \mathbf{T}_{nj}\mathbf{1}, \dots, \mathbf{T}_{nI(-n)}\mathbf{1}] = \mathbf{U}_n * (\mathbf{K}_n \mathbf{V}_n)$ minimizes (7) in Section 6.3. More details regarding update of factor matrix \mathbf{A}_n can be found in Section 6.4. Proof of convergence is presented in 6.5. Section 6.6 illustrates computational complexity of SWIFT. More details regarding computing cost matrices are provided in Section 6.7. Details about projection on learned factor matrices, training strategy, SWIFT’s stopping criteria, and hyper-parameter tuning are provided in Section 6.8. More results on classification performance on noisy data is in Section 6.9. Scalability of SWIFT in compare to a direct implementation is discussed in Section 6.10. Effect of various cost matrices on classification task is described in Section 6.11. Finally, additional results on HF Phenotyping can be found in Section 6.12.

6.1 Symbols and Notations

Table 4 presents the symbols and notations used in this paper.

Table 4: Notation and symbols used throughout this paper.

Symbol	Definition
$*$	Element-wise multiplication
\otimes	Kronecker product
\odot	Khatri–Rao product
\oslash	Element-wise division
$\mathcal{X}, \mathbf{X}, \mathbf{x}, x$	Tensor, Matrix, vector, scalar
$\mathbf{X}_{(n)}$	Mode-n Matricization
$\mathbf{A}(\mathbf{i}, :)$	the i -th row of \mathbf{A}
$\mathbf{A}(:, r)$ or \mathbf{a}_r	the r -th column of \mathbf{A}
\mathbf{A}_n	n -th factor matrix
$\mathbf{A}_{\odot}^{(-n)}$	Khatri-Rao product of all factor matrices except the n -th one
$\langle \mathbf{x}, \mathbf{y} \rangle = \mathbf{x}^T \mathbf{y}$	Inner product between \mathbf{x}, \mathbf{y}
$\text{vec}(\mathbf{A})$	converting matrix \mathbf{A} into a vector

6.2 Proof of Proposition 1

For simplicity, we ignore the entropy regularization term ($\frac{1}{\rho} E(\mathbf{T})$) similar to [17]. In order to prove that Wasserstein distance for tensors is a valid metric, we assume that the cost matrix of mode- n ($\mathbf{C}_{(n)} \in \mathbb{R}_+^{I_n \times I_n}$):

- Is symmetric ($\mathbf{C}_{(n)}(i, j) = \mathbf{C}_{(n)}(j, i); \quad \forall i, j$).
- All of its off diagonal elements are positive and non-zero. ($\mathbf{C}_{(n)}(i, j) = 0, \forall i = j$)
- $\mathbf{C}_{(n)}(i, j) \leq \mathbf{C}_{(n)}(i, k) + \mathbf{C}_{(n)}(k, j) \quad \forall i, j, k$

The positivity and symmetry of a distance follow then from

$$W_T(\mathcal{X}, \mathcal{Y}) = \sum_{n=1}^N W_M(\mathbf{X}_{(n)}, \mathbf{Y}_{(n)}) \quad (11a)$$

$$= \sum_{n=1}^N \sum_{i_n=1}^{I_{(-n)}} W_V(\mathbf{x}_{ni_n}, \mathbf{y}_{ni_n}) \quad (11b)$$

$$= \sum_{n=1}^N \sum_{i_n=1}^{I_{(-n)}} \langle \mathbf{C}_{(n)}, \mathbf{T}_{ni_n} \rangle \quad (11c)$$

$$= \sum_{n=1}^N \sum_{i_n=1}^{I_{(-n)}} W_V(\mathbf{y}_{ni_n}, \mathbf{x}_{ni_n}) \quad (11d)$$

$$= \sum_{n=1}^N W_M(\mathbf{Y}_{(n)}, \mathbf{X}_{(n)}) \quad (11e)$$

$$= W_T(\mathcal{Y}, \mathcal{X}) \quad (11f)$$

Here, $\mathbf{x}_{ni_n} \in \mathbb{R}_+^{I_n}$, $\mathbf{y}_{ni_n} \in \mathbb{R}_+^{I_n}$ are probability vectors and $\|\mathbf{x}_{ni_n}\|_1 = \|\mathbf{y}_{ni_n}\|_1 = 1$. (11a) and (11b) are expanded based on Definitions 2, 1. (11c) is written based on the definition of Wasserstein distance for two vectors. (11d) is written based on the fact that \mathbf{C}_n is a symmetric matrix $\forall n$. Similarly, (11e) and (11f) are written based on Definitions 1, 2. These equations show that Wasserstein distance for two tensors is symmetric. The proof of positivity is straightforward, since all the off diagonal elements of $\mathbf{C}_{(n)}$ are positive, therefore $\langle \mathbf{C}_{(n)}, \mathbf{T}_{ni_n} \rangle > 0 \quad \forall i_n, n$ which suggests $W_T(\mathcal{X}, \mathcal{Y}) > 0$.

To prove the triangle inequality of Wasserstein distances for tensors we know that

$$W_T(\mathcal{X}, \mathcal{Y}) = \sum_{n=1}^N \sum_{i_n=1}^{I_{(-n)}} W_V(\mathbf{x}_{ni_n}, \mathbf{y}_{ni_n}) \quad (12)$$

$$W_T(\mathcal{X}, \mathcal{Z}) = \sum_{n=1}^N \sum_{i_n=1}^{I_{(-n)}} W_V(\mathbf{x}_{ni_n}, \mathbf{z}_{ni_n}) \quad (13)$$

$$W_T(\mathcal{Z}, \mathcal{Y}) = \sum_{n=1}^N \sum_{i_n=1}^{I_{(-n)}} W_V(\mathbf{z}_{ni_n}, \mathbf{y}_{ni_n}) \quad (14)$$

We already know that triangle inequality of Wasserstein distances for every three probability vectors holds [17, 25] which means:

$$\forall \mathbf{x}_{ni_n}, \mathbf{y}_{ni_n}, \mathbf{z}_{ni_n} \quad W_V(\mathbf{x}_{ni_n}, \mathbf{y}_{ni_n}) \leq W_V(\mathbf{x}_{ni_n}, \mathbf{z}_{ni_n}) + W_V(\mathbf{z}_{ni_n}, \mathbf{y}_{ni_n}) \quad (15)$$

By knowing this fact we can extend it to every triple of tensors $(\mathcal{X}, \mathcal{Y}, \mathcal{Z})$ where their unfolding includes probability vectors:

$$W_T(\mathcal{X}, \mathcal{Y}) \leq W_T(\mathcal{X}, \mathcal{Z}) + W_T(\mathcal{Z}, \mathcal{Y}) \quad (16)$$

6.3 Proof of Proposition 2

Here, we follow the same strategy as [18]. \mathbf{T}_{nj} is the optimal transport matrix between $\widehat{\mathbf{X}}_{(n)}(:, j)$, $\mathbf{X}_{(n)}(:, j)$ in mode-n. In order to compute the \mathbf{T}_{nj} , we need to take the derivative with respect to (7).

$$\frac{\partial W_T(\mathcal{X}, \widehat{\mathcal{X}})}{\partial \mathbf{T}_{nj}(i, k)} = \frac{\partial \left(\langle \overline{\mathbf{C}}_n, \overline{\mathbf{T}}_n \rangle - \frac{1}{\rho} E(\overline{\mathbf{T}}_n) + \lambda \left(KL(\Delta(\overline{\mathbf{T}}_n) \| \widehat{\mathbf{X}}_{(n)}) + KL(\Psi(\overline{\mathbf{T}}_n) \| \mathbf{X}_{(n)}) \right) \right)}{\partial \mathbf{T}_{nj}(i, k)} = 0$$

$$\begin{aligned}
 &\Rightarrow \mathbf{C}_n(i, k) + \frac{1}{\rho}(\log(\mathbf{T}_{nj}(i, k)) + 1) + \lambda \log\left(\mathbf{T}_{nj}\mathbf{1} \oslash \widehat{\mathbf{X}}_{(n)}(:, j)\right)_i + \lambda \log\left(\mathbf{T}_{nj}^T\mathbf{1} \oslash \mathbf{X}_{(n)}(:, j)\right)_k = 0 \\
 &\Rightarrow \log(\mathbf{T}_{nj}(i, k)) + \lambda \rho \left(\log\left(\mathbf{T}_{nj}\mathbf{1} \oslash \widehat{\mathbf{X}}_{(n)}(:, j)\right)_i + \log\left(\mathbf{T}_{nj}^T\mathbf{1} \oslash \mathbf{X}_{(n)}(:, j)\right)_k \right) = -\rho \mathbf{C}_n(i, k) - 1 \\
 &\Rightarrow \mathbf{T}_{nj}(i, k) * \left(\left(\mathbf{T}_{nj}\mathbf{1} \oslash \widehat{\mathbf{X}}_{(n)}(:, j) \right)_i^{\lambda \rho} \left(\mathbf{T}_{nj}^T\mathbf{1} \oslash \mathbf{X}_{(n)}(:, j) \right)_k^{\lambda \rho} \right) = \exp(-\rho \mathbf{C}_n(i, k) - 1) \\
 &\Rightarrow \mathbf{T}_{nj}(i, k) = \left(\widehat{\mathbf{X}}_{(n)}(:, j) \oslash \mathbf{T}_{nj}\mathbf{1} \right)_i^{\lambda \rho} \left(\mathbf{X}_{(n)}(:, j) \oslash \mathbf{T}_{nj}^T\mathbf{1} \right)_k^{\lambda \rho} \exp(-\rho \mathbf{C}_n(i, k) - 1)
 \end{aligned}$$

Therefore, $\mathbf{T}_{nj} = \text{diag}(\mathbf{u}_j) \mathbf{K}_n \text{diag}(\mathbf{v}_j)$ where $\mathbf{u}_j = (\widehat{\mathbf{X}}_{(n)}(:, j) \oslash \mathbf{T}_{nj}\mathbf{1})^{\lambda \rho} \in \mathbb{R}^{I_n}$ and $\mathbf{v}_j = (\mathbf{X}_{(n)}(:, j) \oslash \mathbf{T}_{nj}^T\mathbf{1})^{\lambda \rho} \in \mathbb{R}^{I_n}$ and $\mathbf{K}_n = e^{(-\rho \mathbf{C}_n - 1)}$ where \oslash represents element-wise division.

$$\begin{aligned}
 \mathbf{T}_{nj}\mathbf{1} &= \text{diag}(\mathbf{u}_j) \mathbf{K}_n \mathbf{v}_j = \mathbf{u}_j * (\mathbf{K}_n \mathbf{v}_j) = (\widehat{\mathbf{X}}_{(n)}(:, j) \oslash \mathbf{T}_{nj}\mathbf{1})^{\lambda \rho} * (\mathbf{K}_n \mathbf{v}_j) \\
 &\Rightarrow (\mathbf{T}_{nj}\mathbf{1})^{(\lambda \rho + 1)} = (\widehat{\mathbf{X}}_{(n)}(:, j))^{\lambda \rho} * (\mathbf{K}_n \mathbf{v}_j) \\
 &\Rightarrow \text{diag}(\mathbf{u}_j) (\mathbf{K}_n \mathbf{v}_j)^{(\lambda \rho + 1)} = \text{diag}(\widehat{\mathbf{X}}_{(n)}(:, j))^{\lambda \rho} (\mathbf{K}_n \mathbf{v}_j) \\
 &\Rightarrow \mathbf{u}_j^{(\lambda \rho + 1)} = (\widehat{\mathbf{X}}_{(n)}(:, j))^{\lambda \rho} * (\mathbf{K}_n \mathbf{v}_j)^{(-\lambda \rho)} \\
 &\Rightarrow \mathbf{u}_j = (\widehat{\mathbf{X}}_{(n)}(:, j))^{\frac{\lambda \rho}{\lambda \rho + 1}} * (\mathbf{K}_n \mathbf{v}_j)^{\frac{-\lambda \rho}{(\lambda \rho + 1)}} \\
 &\Rightarrow \mathbf{U}_n = [\mathbf{u}_1, \dots, \mathbf{u}_j, \dots, \mathbf{u}_{I(-n)}] = (\widehat{\mathbf{X}}_{(n)})^{\frac{\lambda \rho}{\lambda \rho + 1}} * (\mathbf{K}_n \mathbf{V}_n)^{\frac{-\lambda \rho}{(\lambda \rho + 1)}} = (\widehat{\mathbf{X}}_{(n)})^{\frac{\lambda \rho}{\lambda \rho + 1}} \oslash (\mathbf{K}_n \mathbf{V}_n)^{\frac{\lambda \rho}{(\lambda \rho + 1)}}
 \end{aligned}$$

By applying the similar procedure $\mathbf{V}_n = (\mathbf{X}_{(n)})^{\frac{\lambda \rho}{\lambda \rho + 1}} \oslash (\mathbf{K}_n^T \mathbf{U}_n)^{\frac{\lambda \rho}{(\lambda \rho + 1)}}$. Therefore, $\mathbf{U}_n = (\widehat{\mathbf{X}}_{(n)})^\Phi \oslash (\mathbf{K}_n (\mathbf{X}_{(n)} \oslash (\mathbf{K}_n^T \mathbf{U}_n))^\Phi)^\Phi$ where $\Phi = \frac{\lambda \rho}{\lambda \rho + 1}$.

By knowing $\mathbf{T}_{nj}\mathbf{1} = \mathbf{u}_j * (\mathbf{K}_n \mathbf{v}_j)$ we can extend $\Delta_n = [\mathbf{T}_{n1}\mathbf{1}, \dots, \mathbf{T}_{nj}\mathbf{1}, \dots, \mathbf{T}_{nI(-n)}\mathbf{1}] = \mathbf{U}_n * (\mathbf{K}_n \mathbf{V}_n)$.

6.4 Details on Updating Factor Matrix \mathbf{A}_n

Algorithm 2 presents the pseudo code for updating factor matrix \mathbf{A}_n . As we mentioned earlier, operator $\Pi(\Delta(\overline{\mathbf{T}}_i), n) \sim \mathbb{R}^{I_i \times I_{(-i)}} \rightarrow \mathbb{R}^{I_n \times I_{(-n)}}$ executes a sequence of reshape, permute, reshape on $\Delta(\overline{\mathbf{T}}_i) \in \mathbb{R}^{I_i \times I_{(-i)}}$ and converts its size to $I_n \times I_{(-n)}$. More specifically, line 2 in Algorithm 2 reshapes matrix $\Delta(\overline{\mathbf{T}}_i) \in \mathbb{R}^{I_i \times I_{(-i)}}$ to tensor $\mathcal{D}_i \in \mathbb{R}^{I_1 \times \dots \times I_{i-1} \times I_{(i+1)} \times \dots \times I_N \times I_i}$. Line 3-9 permute modes i, n in \mathcal{D}_i and map it to $\mathcal{D}_{i \rightarrow n} \in \mathbb{R}^{I_1 \times \dots \times I_{n-1} \times I_{n+1} \times \dots \times I_N \times I_n}$. Depending on the position of i , Lines 3,4 show the permutation when $i < n$, Lines 5,6 show the case when i equals n , and lines 7,8 present the permutation when $i > n$. Here, $\text{idx}(\cdot)$ returns the index of a given mode. For instance, in $[I_1, \dots, I_{i-1}, I_{i+1}, \dots, I_N, I_i]$, $\text{idx}(i-1) = i-1$, $\text{idx}(i) = N$, $\text{idx}(i+1) = i$. In line 10, tensor $\mathcal{D}_{i \rightarrow n}$ reshapes to a matrix with size $I_n \times I_{(-n)}$. Once we apply Π on both right and left hand side of (8), we get the new form as follows:

$$\underset{\mathbf{A}_n \geq 0}{\text{minimize}} \sum_{i=1}^N KL \left(\Pi(\Delta(\overline{\mathbf{T}}_i), n) \parallel \mathbf{A}_n (\mathbf{A}_\odot^{(-n)})^T \right) \quad (17)$$

Now we can easily update \mathbf{A}_n based on a multiplicative update rule [30] with the following form (line 13 in Algorithm 2):

$$\mathbf{A}_n = \mathbf{A}_n * \left(\left(\sum_{i=1}^N \Pi(\Delta(\overline{\mathbf{T}}_i), n) \oslash \mathbf{A}_n (\mathbf{A}_\odot^{(-n)})^T \right) \mathbf{A}_\odot^{(-n)} \right) \oslash \mathbf{1} \mathbf{A}_\odot^{(-n)} \quad (18)$$

6.5 Proof of Proposition 3

Consider SWIFT's objective function:

$$\underset{\{\mathbf{A}_n \geq 0, \overline{\mathbf{T}}_n\}_{n=1}^N}{\text{minimize}} \sum_{n=1}^N \left(\underbrace{\langle \overline{\mathbf{C}}_n, \overline{\mathbf{T}}_n \rangle - \frac{1}{\rho} E(\overline{\mathbf{T}}_n)}_{\text{Part } P_1} + \underbrace{\lambda \left(KL(\Delta(\overline{\mathbf{T}}_n) \parallel \mathbf{A}_n (\mathbf{A}_\odot^{(-n)})^T) \right)}_{\text{Part } P_2} + \underbrace{KL(\Psi(\overline{\mathbf{T}}_n) \parallel \mathbf{X}_{(n)})}_{\text{Part } P_3} \right) \quad (19)$$

Algorithm 2 Updating Factor Matrix \mathbf{A}_n

Input: $\Delta(\bar{\mathbf{T}}_i) \in \mathbb{R}^{I_i \times I_{(-i)}} \quad \forall i = 1, \dots, N, \text{ mode-}n, \mathbf{P} = \mathbf{A}_n(\mathbf{A}_{\odot}^{(-n)})^T$
Output: $\mathbf{A}_n \in \mathbb{R}^{I_n \times R}$

```

1: for  $i=1, \dots, N$  do
    //reshape a matrix to a tensor.
2:    $\mathcal{D}_i = \text{reshape}(\Delta(\bar{\mathbf{T}}_i), [I_1, \dots, I_{(i-1)}, I_{(i+1)}, \dots, I_N, I_i])$ 
    //interchange the  $i$ -th and  $n$ -th modes of the tensor.
3:   if  $(i < n)$  then
4:      $\mathcal{D}_{i \rightarrow n} = \text{Permute}(\mathcal{D}_i, [\text{idx}(1), \dots, \text{idx}(i-1), \text{idx}(i), \text{idx}(i+1), \dots, \text{idx}(n-1), \text{idx}(n+1), \dots, \text{idx}(N), \text{idx}(n)])$ 
5:   else if  $(i == n)$  then
6:      $\mathcal{D}_{i \rightarrow n} = \mathcal{D}_i$ 
7:   else
8:      $\mathcal{D}_{i \rightarrow n} = \text{Permute}(\mathcal{D}_i, [\text{idx}(1), \dots, \text{idx}(n-1), \text{idx}(n+1), \dots, \text{idx}(i-1), \text{idx}(i), \text{idx}(i+1), \dots, \text{idx}(N), \text{idx}(n)])$ 
9:   end if
    //reshape a tensor to a matrix.
10:   $\Pi(\Delta(\bar{\mathbf{T}}_i), n) = \text{reshape}(\mathcal{D}_{i \rightarrow n}, [I_n, I_{(-n)}])$ 
11:   $\Pi(\mathbf{A}_i(\mathbf{A}_{\odot}^{(-i)})^T, n) = \mathbf{P}$ 
12: end for
13:  $\mathbf{A}_n = \mathbf{A}_n * \left( \left( \sum_{i=1}^N \Pi(\Delta(\bar{\mathbf{T}}_i), n) \odot \mathbf{P} \right) \mathbf{A}_{\odot}^{(-n)} \right) \odot \mathbf{1} \mathbf{A}_{\odot}^{(-n)}$ 

```

The variables in (19) separated into N different optimal transport problems $(\bar{\mathbf{T}}_n)$ and N different factor matrices (\mathbf{A}_n) . We use Block Coordinate Descent (BCD) framework. BCD iteratively solves one variable at a time while fixing others. Therefore, in every step the objective function is minimized with respect to each of the variables [38]. Each sub-problem in (19) is continuous, differentiable, and strictly convex since minimizing the Frobenius inner product, negative entropy, and KL-Divergence are strictly convex problems [39]. Therefore, based on [38], (19) converges to a stationary point.

6.6 Complexity Analysis of SWIFT

Here, we provide the complexity analysis of different parts of SWIFT. In every iteration, we update N different optimal transport problems and N factor matrices based on Algorithm 1.

In order to update n -th optimal transport problem $(\bar{\mathbf{T}}_n)$, we need to compute the following parts: \mathbf{K}_n requires $\mathcal{O}(I_n^2)$ flops (i.e. floating-point operation). Computing $\mathbf{A}_{\odot}^{(-n)}$ needs $\mathcal{O}(I_{(-n)}R)$ and $\hat{\mathbf{X}}_{(n)} = \mathbf{A}_n(\mathbf{A}_{\odot}^{(-n)})^T$ requires $\mathcal{O}(I_1 \dots I_N R)$ flops. The complexity of computing $\mathbf{U}_n = (\hat{\mathbf{X}}_{(n)})^{\Phi} \odot \left(\mathbf{K}_n \left(\mathbf{X}_{(n)} \odot (\mathbf{K}_n^T \mathbf{U}_n) \right)^{\Phi} \right)^{\Phi}$ (line 8 in Algorithm 1) is $\mathcal{O}(I_n^2 N N Z_n)$ where NNZ_n indicates the number of non-zero columns in $\mathbf{X}_{(n)}$. Line 10 in Algorithm 1 $(\mathbf{V}_n = (\mathbf{X}_{(n)} \odot (\mathbf{K}_n^T \mathbf{U}_n))^{\Phi})$ requires $\mathcal{O}(I_n^2 N N Z_n)$ flops and finally computing $\Delta(\bar{\mathbf{T}}_n) = \mathbf{U}_n * (\mathbf{K}_n \mathbf{V}_n)$ involves $\mathcal{O}(I_n^2 N N Z_n)$.

The steps for updating **Factor matrix** n are as follows: Both reshape and permute operations can be done in $\mathcal{O}(N)$. Factor matrix \mathbf{A}_n is updated based on (18) which can be computed in $\mathcal{O}(RI_1 \dots I_N)$ flops. Finally, the total complexity of SWIFT is $\mathcal{O}(RI_1 \dots I_N)$.

6.7 Cost Matrix Calculation

The cost matrices are derived from the same input data without any additional external knowledge.

For BBC NEWS data we compute the following cost matrices:

- Article \times Article:** The articles are converted to a matrix of TF-IDF (term frequency-inverse document frequency) features. Then the cost matrix between articles i, j is computed based on cosine distance $(\mathbf{C}(i, j) = 1 - \frac{\langle \mathbf{a}_i, \mathbf{a}_j \rangle}{\|\mathbf{a}_i\| \|\mathbf{a}_j\|})$ where \mathbf{a}_i is the TF-IDF vector of article i .
- Word \times Word:** For each word, we construct a multi-hot encoding vector with the size of documents in the training set. Then we define the cost matrix as the cosine distance between every pair of vectors.

The cost matrices in H1 data are:

- **Patient \times Patient:** For each patient we create a vector by concatenating diagnosis and medication features and use cosine distance to compute the cost matrix.
- **Diagnosis \times Diagnosis:** We represent each diagnosis as a multi-hot encoding vector with the size of patients in the training set. If a patient have a certain diagnosis then its corresponding value is one, zero otherwise. We use cosine distance to calculate the cost matrix between every pair of diagnosis vectors.
- **Medication \times Medication:** We perform a similar computation as the Diagnosis \times Diagnosis cost matrix. Note that for **Similarity based CP** [15], we use the same cost matrices.

6.8 Q1. Classification Performance of SWIFT.

Projection on Learned Factor Matrices Given the learned factor matrices ($\mathbf{A}_{train_2}, \dots, \mathbf{A}_{train_N}$) from training data, SWIFT is able to project the new unseen data $\mathcal{X}_{new} \in \mathbb{R}^{I_{new_1} \times I_2 \times \dots \times I_N}$ into existing factors and learn \mathbf{A}_{new_1} .

$$\begin{aligned} & \underset{\{\bar{\mathbf{T}}_n\}_{n=1}^N, \mathbf{A}_{new_1} \geq 0}{\text{minimize}} && \sum_{n=1}^N \left(\langle \bar{\mathbf{C}}_n, \bar{\mathbf{T}}_n \rangle - \frac{1}{\rho} E(\bar{\mathbf{T}}_n) \right) \\ & \text{Subject to} && \bar{\mathbf{T}}_n \in U(\mathbf{X}_{new(n)}, \hat{\mathbf{X}}_{new(n)}) \quad \forall n = 1, \dots, N, \\ & && \hat{\mathcal{X}} = \llbracket \mathbf{A}_{new_1}, \mathbf{A}_{train_2} \dots, \mathbf{A}_{train_N} \rrbracket, \end{aligned} \quad (20)$$

Here, we need to minimize (20) with respect to $\bar{\mathbf{T}}_n$, for $n = 1, \dots, N$ and \mathbf{A}_{new_1} while $\mathbf{A}_{train_2}, \dots, \mathbf{A}_{train_N}$ are fixed. After learning \mathbf{A}_{new_1} , we pass it to Lasso Logistic Regression to predict the labels. We use (20) for projecting the validation and test data.

Training Strategy: Assume we want to classify the elements in the first factor matrix (\mathbf{A}_1) (e.g. article mode for BBC News and patient mode for H1). For all the approaches under the comparison, we use a similar training strategy with the following steps: 1) we split tensor \mathcal{X} from it's first mode into training, validation, and test sets by a ratio of 3:1:1 and construct tensors (\mathcal{X}_{train}), (\mathcal{X}_{val}), and (\mathcal{X}_{test}). 2) We train the factorization model using the training set (\mathcal{X}_{train}) and compute \mathbf{A}_{train_n} $n = 1, \dots, N$. Note that in this step, the label information is not used (except for the baseline Supervised CP, which use label information in the factorization step). 3) Then we freeze the factor matrices of all modes except the one with label information (article mode for BBC News and patient mode for H1), and project the validation and test sets onto the learned factor matrices to obtain the factor matrix of the mode with labels for the test set based on Equation(20). 4) Finally we use a lasso logistic regression to perform the classification. We used a five-fold cross validation.

SWIFT Stopping Criteria In order to provide scalable solutions, SWIFT never directly computes transport matrices, therefore, it is expensive to compute the value of its objective function. Similar to [18, 17, 21], we set the number of fixed-point iterations to an arbitrary number. Stopping criterion is set to 50 iterations and Sinkhorn iteration to 25.

Setting hyper-parameters: For SWIFT, we execute a grid search for $\lambda \in \{0.1, 1, 10\}$ and $\rho \in \{10, 20, 50, 100, 1000\}$ and regularization parameter for lasso logistic regression ($\eta \in \{1e-2, 1e-1, 1, 10, 100, 1000, 10000\}$). The hyper-parameters of other baselines including parameter η are carefully tuned for each dataset.

6.9 Q2. Performance on Noisy H1 Data

Classification Performance on Noisy Input: Figure (3) presents the average and standard deviation of PR-AUC Score of heart failure prediction on test data in H1 data set for five-fold cross validation with respect to different levels of noise ($\{0.05, 0.1, 0.15, 0.20, 0.25, 0.30\}$). SWIFT performs better under various noise levels and relatively improves the PR-AUC score over the best baseline by up to 17%.

6.10 Scalability of SWIFT on BBC NEWS and H1 data sets

In this section, we answer the following question: **Q:** How scalable is SWIFT more compared to a direct implementation?

Baseline Construction: We implement a direct version of Wasserstien tensor factorization for 3-order tensors where for optimal transport computation we do not leverage sparsity structure. For updating factor matrix \mathbf{A}_n in the direct version of Wasserstien tensor factorization we move \mathbf{A}_n into a similar position by vectorizing every $\Delta(\mathbf{T}_i)$ and \mathbf{A}_n and rearranged the terms using the properties of Khatri-Rao and Kronecker products, so that \mathbf{A}_n has the same position in all N different KL-divergence terms. We directly utilize Equations (21),(22), (23) to update \mathbf{A}_1 , \mathbf{A}_2 , and \mathbf{A}_3 , respectively. Note that direct Wasserstein TF returns the same solution given the same initialization as to SWIFT.

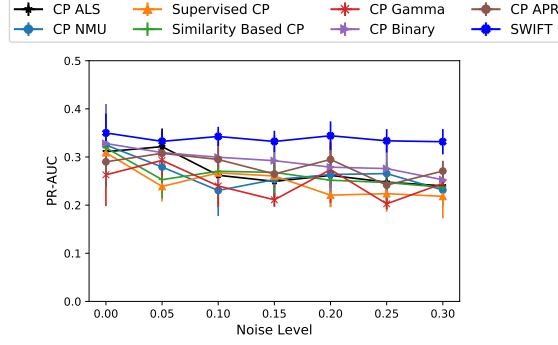


Figure 3: The average and standard deviation of PR-AUC score of different baselines as a function of the noise level on H1 data set.

Each of these objective functions are equivalent to (8), (10) but requires more computation.

$$\underset{\mathbf{A}_1 \geq 0}{\text{minimize}} \quad KL \left(\begin{bmatrix} \text{vec}(\Delta(\mathbf{T}_1)) \\ \text{vec}(\Delta(\mathbf{T}_2)^T) \\ \text{vec}(\Delta(\mathbf{T}_3)^T) \end{bmatrix} \parallel \begin{bmatrix} (\mathbf{A}_3 \odot \mathbf{A}_2) \otimes \mathbf{I}_{I_1} \\ (\mathbf{A}_2 \otimes \mathbf{I}_{I_3 I_1})((\mathbf{I}_R \odot \mathbf{A}_3) \otimes \mathbf{I}_{I_1}) \\ (\mathbf{A}_3 \otimes \mathbf{I}_{I_2 I_1})(\mathbf{I}_R \odot \mathbf{A}_2) \otimes \mathbf{I}_{I_1} \end{bmatrix} \text{vec}(\mathbf{A}_1) \right) \quad (21)$$

$$\underset{\mathbf{A}_2 \geq 0}{\text{minimize}} \quad KL \left(\begin{bmatrix} \text{vec}(\Delta(\mathbf{T}_1)^T) \\ \text{vec}(\Delta(\mathbf{T}_2)) \\ \text{vec}(\Delta(\mathbf{T}_3)^T) \end{bmatrix} \parallel \begin{bmatrix} (\mathbf{A}_1 \otimes \mathbf{I}_{I_3 I_2})((\mathbf{I}_R \odot \mathbf{A}_3) \otimes \mathbf{I}_{I_2}) \\ (\mathbf{A}_3 \odot \mathbf{A}_1) \otimes \mathbf{I}_{I_2} \\ (\mathbf{A}_3 \otimes \mathbf{I}_{I_1 I_2})(\mathbf{I}_{I_2 R} \odot (\mathbf{A}_1(\mathbf{I}_R \otimes \mathbf{1}_{1 \times I_2}))) \end{bmatrix} \text{vec}(\mathbf{A}_2) \right) \quad (22)$$

$$\underset{\mathbf{A}_3 \geq 0}{\text{minimize}} \quad KL \left(\begin{bmatrix} \text{vec}(\Delta(\mathbf{T}_1)^T) \\ \text{vec}(\Delta(\mathbf{T}_2)^T) \\ \text{vec}(\Delta(\mathbf{T}_3)) \end{bmatrix} \parallel \begin{bmatrix} (\mathbf{A}_1 \otimes \mathbf{I}_{I_3 I_2}) \left(\begin{bmatrix} \mathbf{I}_{I_3 R} \odot (\mathbf{A}_2(\mathbf{I}_R \otimes \mathbf{1}_{1 \times I_3})) \\ \mathbf{I}_{I_3 R} \odot (\mathbf{A}_1(\mathbf{I}_R \otimes \mathbf{1}_{1 \times I_2})) \end{bmatrix} \right) \\ (\mathbf{A}_2 \otimes \mathbf{I}_{I_3 I_1}) \left(\begin{bmatrix} \mathbf{I}_{I_3 R} \odot (\mathbf{A}_1(\mathbf{I}_R \otimes \mathbf{1}_{1 \times I_2})) \\ (\mathbf{A}_2 \odot \mathbf{A}_1) \otimes \mathbf{I}_{I_3} \end{bmatrix} \right) \end{bmatrix} \text{vec}(\mathbf{A}_3) \right) \quad (23)$$

We can easily prove that equations (21), (22), (23) are equivalent to (8), (10) by knowing the following properties:

1. $KL(\mathbf{A} \parallel \mathbf{B}) = KL(\text{vec}(\mathbf{A}) \parallel \text{vec}(\mathbf{B}))$
2. $KL(\mathbf{A} \parallel \mathbf{B}) = KL(\mathbf{A}^T \parallel \mathbf{B}^T)$
3. $(\mathbf{E}^T \otimes \mathbf{C})\text{vec}(\mathbf{D}) = \text{vec}(\mathbf{CDE})$ [40]
4. $\text{vec}(\mathbf{A}_3 \odot \mathbf{A}_2) = ((\mathbf{I}_R \odot \mathbf{A}_3) \otimes \mathbf{I}_{I_2})\text{vec}(\mathbf{A}_2)$ [41].
5. $\text{vec}(\mathbf{A}_2 \odot \mathbf{A}_1) = (\mathbf{I}_{I_2 R} \odot (\mathbf{A}_1(\mathbf{I}_R \otimes \mathbf{1}_{1 \times I_2})))\text{vec}(\mathbf{A}_2)$ [41].
6. $\mathbf{I}_{I_1 I_2} = (\mathbf{I}_{I_1} \otimes \mathbf{I}_{I_2}) = (\mathbf{I}_{I_2} \otimes \mathbf{I}_{I_1}) = \mathbf{I}_{I_2 I_1}$ [40].

Results: In Figure 4, we vary 1) size of a mode, 2) target rank (R), and 3) number of Sinkhorn iterations in optimal transport problems and report the average and standard deviation of running time (in seconds) for one iteration as an average of five different runs for H1 and BBC NEWS data sets.

Figure (4a) depicts the time as we increase the number of patients ($\{500, 750, 1000, 1250\}$). SWIFT is up to $293\times$ faster than the Wasserstein TF model. Execution in the direct Wasserstein TF failed for a tensor of $1250 \times 100 \times 100$, due to the excessive amount of memory needed. Next, we compare the scalability of both methods by varying the value for R on Figure (4b). SWIFT achieves up to $928\times$ faster computation. Figure (4c) depicts the optimal transport time² for SWIFT and Wasserstein TF for a tensor with size $1500 \times 500 \times 500$. Generally, more Sinkhorn iterations lead to a better solution for the optimal transport problems. We increase the value of Sinkhorn iterations and SWIFT achieves up to $12\times$ speed up over Wasserstein TF suggests that speedup strategies introduced in Section (3.3) are beneficial.

Next, we perform the experiments for BBC NEWS data. Figure (4d) demonstrates the running time for one iteration as we increase the number of articles in BBC NEWS data ($\{500, 750, 1000, 1250\}$). SWIFT is up to $97\times$ faster than the direct Wasserstien tensor factorization model in Figure (4d). Same as before, execution in the direct Wasserstien TF failed for a tensor of $1250 \times 100 \times 100$, due to the excessive amount of memory. We measure the scalability of both

²We avoid updating factor matrices here and just record the running time of optimal transport problem.

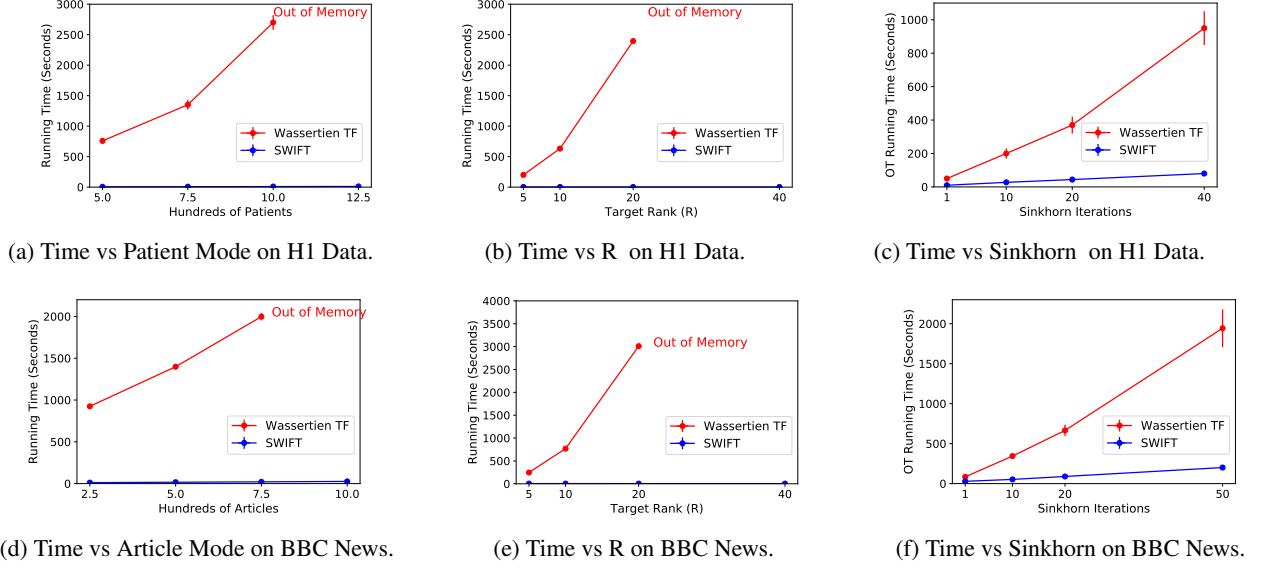


Figure 4: Average and standard deviation of running time in seconds for one iteration (as an average of five) on H1 and BBC NEWS Data sets by increasing 1) a mode size 2) target rank (R) 3) Sinkhorn iteration. For Figures 4c, 4f we report OT running time and for the rest we present the total running time for one iteration. In Figure 4a for 1250 patients and Figure 4b for $R = 40$, Figure 4d for 1000 articles, and Figure 4e, execution in Wasserstien TF (direct baseline) failed due to the excessive amount of memory request.

methods by varying the value for R ($R = \{5, 10, 20, 40\}$) on Figure (4e) where *SWIFT* achieves up to $718\times$ faster computation. Again for $R = 40$, direct Wasserstien TF failed to execute due to out of memory. Finally, Figure (4f) represents the optimal transport running time² for one iteration (as an average of 5) for *SWIFT* and Wasserstien tensor factorization for a tensor with size $1500 \times 500 \times 500$. We increase the value of Sinkhorn iterations ($\{1, 10, 20, 50\}$). *SWIFT* achieves up to $10\times$ speed up over Wasserstien tensor factorization.

Figure (4) suggests the strategies we introduced in Sections (3.3), (3.4) are beneficial and significantly reduce the running time of *SWIFT* in compare to the direct implementation.

6.11 Effect of Cost Matrix on Classification Performance

In order to understand the power of cost matrix (C) on classification performance, we compare different cost matrices including the one we introduced in section 6.7, random and 1-identity (matrix of ones with a zero diagonal) cost matrices for both BBC NEWS and H1 datasets. When the cost matrix is 1-identity then Wasserstien distance can be seen as total variation distance [42].

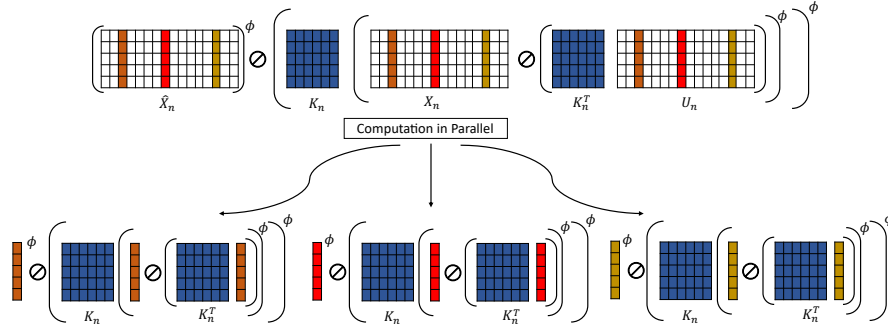
From Table 5 we summarize our observations as follow : 1) using random cost matrices drop the performance. 2) 1-identity cost matrix performs better than random cost matrices but still not as good as cost matrices introduced in Section (6.7). As you can see *SWIFT* with 1-identity cost matrices have better performance than other well-known CP baselines (Comparing with Table 1).

Table 5: Average and standard deviation of accuracy on BBC NEWS and PR-AUC score on H1 data sets by considering different cost matrices for different values of target-rank ($R = [5, 10, 20, 30, 40]$).

		R=5	R=10	R=20	R=30	R=40
BBC NEWS Data	SWIFT (Random)	.621 \pm .041	.693 \pm .053	.684 \pm .038	.712 \pm .047	.684 \pm .022
	SWIFT (1-Identity)	.709 \pm .016	.775 \pm .019	.793 \pm .032	.775 \pm .023	.771 \pm .013
	SWIFT	.759 \pm .013	.781 \pm .013	.803 \pm .010	.815 \pm .005	.818 \pm .022
H1 Data	SWIFT (Random)	.340 \pm .103	.347 \pm .091	.341 \pm .083	.352 \pm .041	.354 \pm .074
	SWIFT (1-Identity)	.363 \pm .105	.349 \pm .079	.344 \pm .073	.358 \pm .063	.368 \pm .074
	SWIFT	.364 \pm .063	.350 \pm .031	.350 \pm .040	.369 \pm .066	.374 \pm .044

Table 6: The phenotypes positively associated with HF. All phenotypes are annotated and endorsed by a medical expert. The remaining phenotypes are whether negatively or none associated with HF.

HF with long-term Diabetes (Weight= 14.62)	HF with Dysrhythmias (Weight= 13.73)
Dx-Diabetes with ketoacidosis or uncontrolled diabetes Dx-Other mycoses Dx-Diabetes mellitus without complication [49.] Rx-Corticosteroids - Topical Rx-Biguanides Rx-Central Muscle Relaxants	Dx-Cardiac dysrhythmias [106.] Dx-Diabetes mellitus without complication [49.] Dx-Other viral infections [7.] Rx-Coumarin Anticoagulants Rx-Gout Agents Rx-Calcium Channel Blockers
CAD related HF (Weight= 10.04)	Aging and frail related HF (Weight= 9.72)
Dx-Cardiac dysrhythmias [106.] Dx-Acute cerebrovascular disease [109.] Dx-Disorders of lipid metabolism [53.] Rx-Coumarin Anticoagulants Rx-Oil Soluble Vitamins Rx-HMG CoA Reductase Inhibitors	Dx-Urinary tract infections [159.] Dx-Genitourinary symptoms and ill-defined conditions [163.] Dx-Other bone disease and musculoskeletal deformities [212.] Rx-Urinary Anti-infectives Rx-Fluoroquinolones Rx-Anti-infective Misc. - Combinations
HF with Pulmonary disease (Weight= 9.58)	HF with air pathway blockage (Weight= 8.98)
Dx-Other and unspecified asthma Dx-Chronic airway obstruction; not otherwise specified Dx-Acute bronchitis [125.] Rx-Sympathomimetics Rx-Fluoroquinolones Rx-Opioid Combinations	Dx-Essential hypertension [98.] Dx-Allergic reactions [253.] Dx-Esophageal disorders [138.] Rx-Calcium Channel Blockers Rx-Beta Blockers Cardio-Selective Rx-Proton Pump Inhibitors
HF with systematic inflammation (Weight= 6.45)	HF with thyroid dysfunction (Weight= 4.08)
Dx-Essential hypertension [98.] Dx-Chronic kidney disease [158.] Dx-Disorders of lipid metabolism [53.] Rx-ACE Inhibitors Rx-HMG CoA Reductase Inhibitors Rx-Calcium Channel Blockers	Dx-Immunizations and screening for infectious disease [10.] Dx-Essential hypertension [98.] Dx-Other thyroid disorders Rx-Antihypertensive Combinations Rx-Impotence Agents Rx-Angiotensin II Receptor Antagonists


 Figure 5: SWIFT explores sparsity structure in input data $X_{(n)}$ and drop zero values columns. Also SWIFT parallelize optimal transport problems for each factor matrix A_n . NNZ_n in this toy example equals 3.

6.12 More Results on HF Phenotyping

Figure 5 depicts the second and third strategies introduced in Section (3.3) in more details.